Accepted Manuscript

On the roles of close shell interactions in the structure of acyl-substituted hydrazones: An experimental and theoretical approach

Aamer Saeed, M. Ifzan Arshad, Michael Bolte, Adolfo C. Fantoni, Zuly Yuliana Delgado Espinoza, Mauricio F. Erben

On the Roles of Close Shell Interactions in the Structure of Acyl-substituted Hydrazones:

an Experimental and Theoretical Approach

Aamer Saeed,[a]* M. Ifzan Arshad,[a] Michael Bolte,[b] Adolfo C. Fantoni,[c] Zuly Yuliana Delgado Espinoza,[d] Mauricio F. Erben [d,*]

[a] *Department of Chemistry, Quaid-I-Azam University, Islamabad 45320, Pakistan.*

[b] *Institut für Anorganische Chemie, J.W.-Goethe-Universität, Max-von-Laue-Str. 7, D-60438 Frankfurt/Main, Germany.*

[c] *Instituto de Física La Plata (UNLP-CONICET), Departamento de Física, Facultad de Ciencias Exactas, Universidad Nacional de La Plata, 49 y 115, La Plata, Buenos Aires, República Argentina.*

[d] *CEQUINOR (UNLP, CONICET-CCT La Plata), Departamento de Química, Facultad de Ciencias Exactas, Universidad Nacional de La Plata, C.C. 962 (1900). La Plata, Buenos Aires, República Argentina.*

* Corresponding authors: (AS) E-mail: aamersaeed@yahoo.com, Tel: +92-51-90642128; Fax: +92-51-90642241. (MFE) E-mail: erben@quimica.unlp.edu.ar, Tel/Fax: +54-211-4259485.

Abstract

The 2-(phenyl-hydrazono)-succinic acid dimethyl ester compound was synthesized by reacting phenylhydrazine with dimethylacetylene dicarboxylate at room temperature and characterized by elemental analysis, infrared, Raman, ^{1}H and ^{13}C NMR spectroscopies and mass spectrometry. Its solid state structure was determined by X-ray diffraction methods. The X-ray structure determination corroborates that the molecule is present in the crystal as the hydrazone tautomer, probably favored by a strong intramolecular N–H···O=C hydrogen bond occurring between the carbonyl (–C=O) and the hydrazone –C=N–NH– groups. A substantial fragment of the molecular skeleton is planar due to an extended π-bonding delocalization. The topological analysis of the electron densities (Atom in Molecule, AIM) allows to characterize intramolecular N–H···O interaction, that can be classified as a resonant assisted hydrogen bond (RAHB). Moreover, the Natural Bond Orbital population analysis confirms that a strong hyperconjugative lpO1→σ*(N2–H) remote interaction between the C2=O1 and N2–H groups takes place. Periodic system electron density and topological analysis have been applied to characterize the intermolecular interactions in the crystal. Weak intermolecular interactions determine the packing and the prevalence of non directional dispersive contributions are inferred on topological grounds. The IR spectrum of the crystalline compound was investigated by means of density functional theory calculations carried out with periodic boundary conditions on the crystal, showing excellent agreement between theory and the experiments. The vibrational assignment is complemented with the analysis of the Raman spectrum.

Keywords: Hydrazone; Crystal structure; FTIR spectroscopy; Raman spectroscopy; Hydrogen bond; NBO; AIM topological analysis

1-Introduction

Hydrazone compounds having the general formula $R^1R^2C=N–NHR^3$ (R= alkyl or aryl groups), are substances formally derived from aldehydes or ketones by reaction with hydrazine or a hydrazine derivative. The hydrazones are well-known compounds for which methods of preparation and structural properties [1] as well as biological aspects [2] were reviewed recently. In particular, these molecular organic compounds have received considerable attention as nonlinear optical materials due to their potentially high nonlinear effects and rapid response in electro-optic devices [3, 4]. For example, the second harmonic generation (SHG) efficieny of benzaldehyde phenylhydrazone was evaluated to be higher than that of urea [5]. It was postulated that the large value of second order hyperpolarizability displayed by this kind of molecules is associated with an Internal Charge Transfer (ICT) process between electron-donor to electron-acceptor groups, facilitated by an extended conjugated π system. In this direction, a family of phenylhydrazono compounds containing the curcumin group was prepared and its structural and electronic properties were determined, showing that the frontier orbital energies are dependent on the electron-donor or electron-withdrawing nature of the substituent groups [6].

Tautormeric equilibria of azo-hydrazone compounds was reported very recently, the azo-enamine tautomer being the predominant form in the solid state, whereas the hydrazone-imine form is the preferred form in solution [7]. Structural properties of salicylhydrazone and aroylhydrazones derived from nicotinic acid hydrazide have been studied [8], the co-existence of

two tautomeric forms was determined for the solid substance, as well as for highly concentrated solutions, whereas only the hydrazone tautomer is present in diluted solutions [9, 10]. It is anticipated that the formation of inter- and intra-molecular hydrogen bonds strongly influence these equilibria [11].

It is an interesting observation that hydrazone species bearing a carbonyl group, i.e. $R^1=$ acyl radical (RC=O, see Scheme 1), are scarcely studied, mostly because the general method for the synthesis of hydrazones failed when the hydrazine is in presence of an electrophilic substituent as the C=O group. Examples include a series of *N*-acylhydrazone compounds with antinociceptive and anti-inflammatory activities synthetized by Barreiro et al. [12], for which the conformational properties in solution were also determined by using NMR data [13]. Regarding structural aspects, the configurational and conformational landscape of 3-oxo-2-(phenylhydrazono) derivatives is influenced by the environment, and a complex interplay between inter- and intra-molecular hydrogen bond interactions was observed in the crystalline structures [14]. Acyl hydrazone compounds bearing also the tetrahydrocabazole group were recently synthesized by Sarıgöl and coworkers [15] and the conformation adopted by the C=O double bond and the hydrazone group was investigated by using quantum chemical calculations. More recently, the tautomeric equilibria of azo-hydrazones dye compounds and their Ni(II) and Cu(II) metal complexes were reported [16-18].

Scheme 1. Representation of acyl substituted hydrazones.

Prompted by this versatile tautomeric and conformational equilibria displayed by hydrazono-carbonyl compounds, we became interested in the study of 2-(phenyl-hydrazono)-succinic acid dimethyl ester (R= CH_3O-, R^2= $CH_3OC(O)CH_2-$, R^3= C_6H_5-, see Scheme 1). Quite recently, this species was postulated as an intermediate in the synthesis of 3,5-di-functionalized pyrazoles [19]. The aim of this work is to provide a comprehensive structural study for this molecule, including the detailed description of the intramolecular and intermolecular interactions in the solid phase, and to determined how these properties influence the vibrational properties. Thus, the preparation, isolation and full characterization is presented, along with the study and analysis of its molecular structure in the crystalline state as determined by single-crystal X-ray diffraction analysis and vibrational spectroscopic techniques (FTIR and FT-Raman). The most salient conformational, tautomeric and configurational properties for the isolated molecule have been studied by using quantum chemical calculations at the B3LYP/6-311++G(d,p) level of approximation. Vibrational frequencies and modes were also calculated at the B3LYP/6-31G** level at the Γ point of the periodic system, after optimization of all atom positions with cell parameters kept at the experimental values. Furthermore, Natural Bond Orbital (NBO) [20] population analysis has been performed in order to evaluate the donor$\rightarrow$ acceptor intramolecular interactions. Since the large number of sites potentially able to establish C–H···O intermolecular interactions makes the system particularly suitable for studying the directional characteristics of this kind of weak interactions and their contribution to crystal packing, we decided to perform an AIM topological analysis of the crystal electron density.

2-Experimental

2.1-General- Melting points were recorded using a digital Gallenkamp (SANYO) model MPD.BM 3.5 apparatus and are uncorrected. ^{1}H and ^{13}C nuclear magnetic resonance (NMR) spectra were determined in CDCl$_3$ at 300 MHz and 75.4 MHz respectively using a Bruker spectrometer. Mass Spectra (EI, 70eV) on a gas chromatography–mass spectrometry (GC-MS) instrument Agilent technologies, and elemental analyses were conducted using a LECO-183 CHNS analyzer. Solid-phase (in KBr pellets) infrared spectra were recorded with a resolution of 2 cm^{-1} in the 4000-400 cm^{-1} range on a Bruker EQUINOX 55 FTIR spectrometer. The FT-Raman spectra of the powdered solid sample were recorded in the region 4000-100 cm^{-1} using a Bruker IFS 66v spectrometer equipped with Nd:YAG laser source operating at 1.064 μm line with 200 mW power of spectral width 2 cm^{-1}.

2.2-Synthesis of 2-(Phenyl-hydrazono)-succinic acid dimethyl ester (3). In a 100 mL two neck round bottom flask, fitted with a reflux condenser, hydrazine (0.22 g, 2 mmol) and dimethyl acetylene dicarboxylate (0.28 g, 2 mmol) were stirred for two hours in 10 mL (1:1) mixture of toluene and dichloromethane. The progress of the reaction was monitored by thin layer chromatography. After the completion of the reaction, the solvent was removed under reduced pressure the residue was extracted with ethyl acetate and water, the organic layer was dried over anhydrous sodium sulphate and concentrated. The crude product was recrystallized from aqueous ethanol. Yield 73%, mp 81°C. FT-IR (ν cm^{-1}): 3268, 3049, 2956, 1739, 1688, 1562, 1437, 1351, 1198, 1164, 1151, 1145, 1000, 791, 691 (see section 3.4 for details). ^{1}H NMR (300 MHz, CDCl$_3$): δ 12.2 (br s, 1H, NH), 7.34-6.91 (m, 5H, Ar H), 3.83 (s, 3H, CO$_2$CH$_3$), 3.74 (s, 3H,

CO$_2$CH$_3$) 3.56 (s, 2H, CH$_2$); ^{13}C NMR (75 MHz, CDCl$_3$): δ 171.4 (C=O), 163.5 (C=O), 142.9 (C=N), 129.3 (ArC), 122.5 (ArC), 121.8 (ArC), 113.9 (ArC), 52.0 (CO$_2$CH$_3$), 51.7 (CO$_2$CH$_3$), 38.9 (CH$_2$). The ^{1}H and ^{13}C NMR spectra are provided as supplementary material (Figures S1 and S2, respectively). Anal. Calcd for C$_{12}$H$_{14}$N$_2$O$_4$: C, 57.59; H, 5.64; N, 11.19; %; Found: C, 57.63; H, 5.61; N, 11.23 %. EIMS (m/z): 250.1 (53%).

2.3-Computational details. Molecular quantum chemical calculations have been performed with the GAUSSIAN 03 program package [21] by using the B3LYP DFT hybrid methods employing Pople-type basis set [22]. The valence triple-ξ basis set augmented with diffuse and polarization functions in both the hydrogen and weighty atoms [6-311++G(d,p)] has been used for geometry optimization and frequency calculations. The calculated vibrational properties corresponded in all cases to potential energy minima for which no imaginary frequency was found. The Potential Energy Distribution PED analysis has been computed using the VEDA4 program [23, 24]. Periodic calculations were performed at the B3LYP/6-31G(d,p) level with Crystal98 and Crystal09 codes [25, 26]. The topology of the resulting electron density was then analyzed using the TOPOND98 program [27]. The whole vibrational data are given as supplementary information in Table S1.

2.4-Crystal structure determination. Data were collected on a STOE IPDS II two-circle diffractometer with a Genix Microfocus tube with mirror optics using Mo$K_α$ radiation ($λ$ = 0.71073 Å) and were scaled using the frame scaling procedure in the *X-AREA* program system [28]. The structure was solved by direct methods using the program SHELXS [29] and refined against F^2 with full-matrix least-squares techniques using the program SHELXL-97 [29]. H atoms bonded to C were refined using a riding model and the H atom bonded to N was freely

refined [28]. Relevant crystallographic data are given as supplementary information in Tables S1-S6. Full crystallographic data have been deposited with the Cambridge Crystallographic Data Centre (CCDC 896977). Enquiries for data can be directed to: Cambridge Crystallographic Data Centre, 12 Union Road, Cambridge, UK, CB2 1EZ or (e-mail) deposit@ccdc.cam.ac.uk or (fax) +44 (0) 1223 336033.

3-Result and discussion

The title compound 2-(phenyl-hydrazono)-succinic acid dimethyl ester was synthesized by slight modification of the literature method [19] using the general Cope-type intermolecular hydroamination of acetylene and hydrazine derivatives reported by Cebrowski et al. [30]. In the present case, equimolar quantities of phenyl hydrazine and dimethylacetylene dicarboxylate (DMAD) in dry toluene and dry dichloromethane, react at room temperature, as outlined in Scheme 2. The crude product was recrystallized from aqueous ethanol.
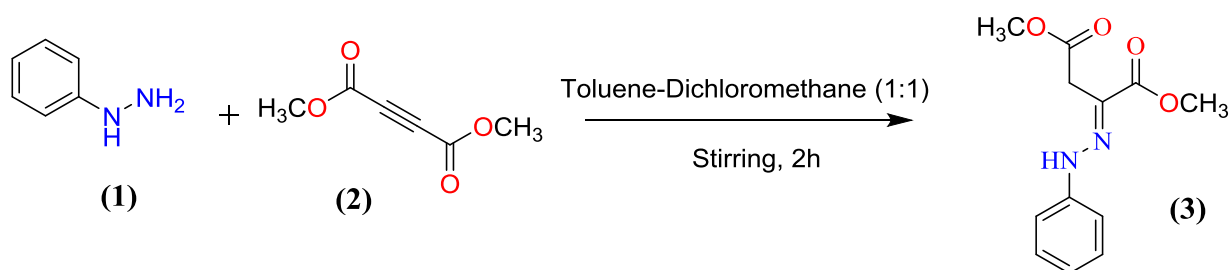
Scheme 2. Synthesis of 2-(Phenyl-hydrazono)-succinic acid dimethyl ester.

The ^{1}H-NMR (300 MHz, CDCl$_3$) data of **(3)** displayed characteristic deshielded singlet at δ= 12.2 ppm for –NH proton, two proton singlet for –CH$_2$– at δ 3.56 ppm, three proton singlets

at δ 3.74 and 3.83 ppm for methyl protons of esters –CO$_2$CH$_3$ and –CH$_2$CO$_2$CH$_3$, respectively, besides the aromatic protons in the range δ= 6.97-7.34 ppm. In the ^{13}C-NMR data of **(3)** signal for –CH$_2$– carbon at δ 38.9 was observed while those at δ= 51.7 and 52.0 ppm correspond to the ester methyl carbons. Additionally, the aromatic carbons appeared at δ 129.3, 122.4, 121.8, and 113.9 (ipso C) and the δ N=C at 122.4 ppm and carbonyls of two ester functionalities were noted at δ=163.6 and 171.4 ppm, respectively. The mass spectral (m/z= 250.1, M$^+$) and elemental analytical data was in full agreement with the assigned structure.

3.1-Tautomerism, configurational and conformational landscape.

The prototropic enolimine–ketoenamine tautomeric and the configurational *E*/*Z* configurational equilibria inherent to Shiff bases, also applies to hydrazone compounds. Miljanić et al. demostrated a complex tautomeric behaviour of aroylhydrazones depending on the state of the sample –DMSO solution or solid- [9]. The position of equilibrium depends considerably also on the nature of substituent groups on the hydrazone moiety [31-33]. In the present case, the relative stability of main tautomers and configurational isomers have been computationally determined by performing full geometry optimization and frequency calculations at the B3LYP/6-311++G(d,p) level of approximation. Three main tautomeric forms were considered, as shown in Figure 1 along with the relative electronic energies (corrected by zero point energy) computed for each form. The hydrazone (ketoenamine) form is strongly favored over the enol-azo (enolimine) form by ca. 38.7 kcal/mol. A third tautomeric form was also considered, which can be formally related with the migration of hydrogen from carbon to nitrogen to form the enamine tautomer [34]. The later is computed to be higher in energy by ca. 9.5 kcal/mol than the

hydrazone form. It is plausible that the formation of the title compound is mediated by a tautomeric equilibria between these last two forms.

Depending on the relative orientation of the substituent around the N1=C1 double bond, two different configurational isomers, e.i. *E* and *Z*, are feasible for the hydrazone form. The *E* form is most stable than the *Z* one by 4.4 kcal/mol. The *E* form allows for the stableshing of a pseudo-six-membered ring between the ester and hydrazo groups, favoring a C2=O1···H–N2 intramolecular hydrogen bond interaction.

Finally, different conformations of the hydrazo-*E* form have been considered, by rotating the C1–C2 single bond, i.e. by changing the mutual orientation of the C=O and C=N double bonds. Two conformations resulted to be minima in the potential energy surface, characterized by the O1/C2/C1/N1 dihedral angle adopting values of 0º and 180º, corresponding to the syn and anti rotamers, respectively. The syn conformer is preferred over the anti one, which is computed higher in energy by 3.8 kcal/mol.

It is worthy to notice that the molecular structure of the most stable form obtained after this computational analysis coincides with the experimental molecular structure derived by X-ray crystallography discussed in the next section. Thus, the obtained geometrical parameters and vibrational data will be discussed in the following sections.
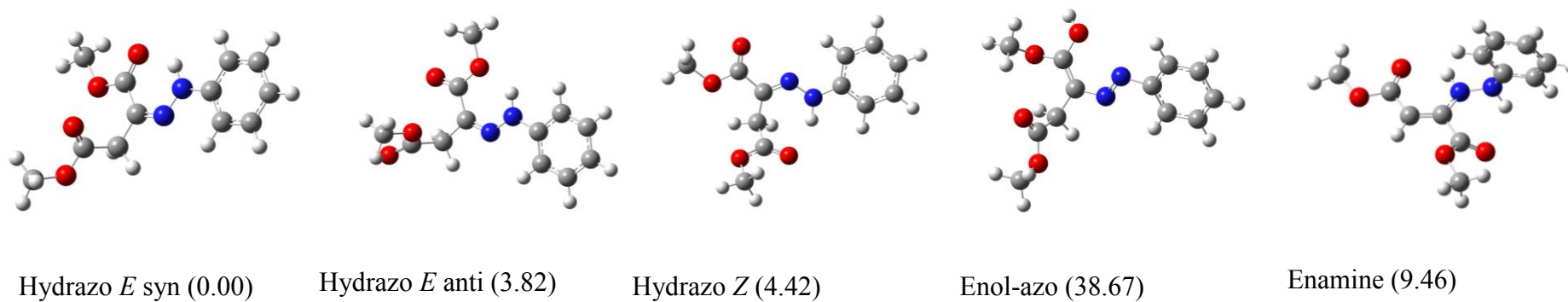
Hydrazo *E* syn (0.00)   Hydrazo *E* anti (3.82)   Hydrazo *Z* (4.42)   Enol-azo (38.67)   Enamine (9.46)

Figure 1. Molecular structures optimized [B3LYP/6-311++G(d,p)] for different tautormers, configurational isomers and conformers of the title species. Relative energies values ($\Delta E°$, in kcal/mol) are given.

3.2-Molecular and crystal structure.

Crystals suitable for X-ray crystallography were obtained by recrystallization from ethanol. The title compound crystallizes in the triclinic centrosymmetric space group (*P*-1) with one molecule in the asymmetric unit. The molecular structure observed in the crystal corresponds to the hydrazo-*E*-syn form computed as the most stable form for the vacuum isolated molecule. An ORTEP drawing of the molecule is shown in Figure 2. Details of crystallographic data refinement are reported in Table 1. The main structural parameters resulting for the molecule are collected in Table 2, where the corresponding values obtained from quantum chemical calculations are also reported for comparison. There is in general good agreement between both sets of structural data, the values being within expected ranges [35]. The overall structure was found to be similar to that of dimethyl 2-[2-(2,4,6-trichlorophenyl)hydrazin-1-ylidene]butanedioate, published recently [36].
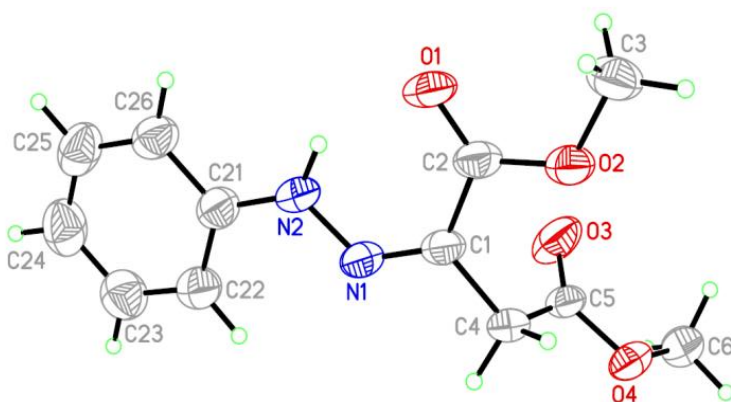

Figure 2. Crystal structure of 2-(Phenyl-hydrazono)-succinic acid dimethyl ester **(3)**.

Table 1. Crystal data and structure refinement for **(3)**.

Empirical formula	$C_{12}H_{14}N_2O_4$
Formula weight	250.25
Temperature	173(2) K
Wavelength	0.71073 Å
Crystal system	Triclinic
Space group	*P*-1
Unit cell dimensions	a = 6.748(2) Å $\quad$ α= 87.02(3)°.
	b = 7.930(3) Å $\quad$ β= 78.35(3)°.
	c = 12.871(4) Å $\quad$ γ = 67.51(3)°.
Volume	623.0(4) Å^3
Z	2
Density (calculated)	1.334 Mg/m^3
Absorption coefficient	0.101 mm^{-1}
F(000)	264
Crystal size	0.37 x 0.24 x 0.04 mm^3
Theta range for data collection	3.33 to 25.77°.
Index ranges	-8<=h<=8, -9<=k<=9, -15<=l<=15
Reflections collected	6803
Independent reflections	2325 [R(int) = 0.1152]
Completeness to theta = 25.00°	99.2 %
Absorption correction	Semi-empirical from equivalents
Max. and min. transmission	0.9960 and 0.9634
Refinement method	Full-matrix least-squares on F^2
Data / restraints / parameters	2325 / 0 / 167
Goodness-of-fit on F^2	1.002
Final R indices [I>2sigma(I)]	R1 = 0.0763, wR2 = 0.1852

R indices (all data)   R1 = 0.1236, wR2 = 0.2101

Largest diff. peak and hole   0.284 and -0.312 e.Å^{-3}

Table 2. Experimental X-ray and calculated [B3LYP/6-311++G(d,p)] selected geometric parameters (Å and º) of the central hydrazone group for **(3)**.

Parameter	Exp	Calc		Parameter	Exp	Calc
C21–N2	1.372(5)	1.402		C21–N2–N1	119.2(3)	121.3
N2–N1	1.347(3)	1.317		N2–N1=C1	121.0(3)	122.1
C1=N1	1.295(4)	1.303		N1=C1C2	125.1(2)	123.1
C1–C2	1.469(4)	1.472		C1–C2=O1	124.8(3)	124.9
C2=O1	1.219(3)	1.223		O2–C2=O1	123.3(3)	122.6
C2–O2	1.336(4)	1.347		C1C4C5	112.9(3)	113.4
C1–C4	1.513(4)	1.504		C4C5=O3	127.1(3)	126.3
C4–C5	1.485(5)	1.521		O4–C5=O3	121.2(3)	123.6
C5=O3	1.203(4)	1.205		N1=C1–C2=O1	3.6(6)	2.4
C5–O4	1.341(3)	1.350		N1=C1–C4–C5	103.7(4)	108.8

The molecular conformation is stabilized by an intramolecular N–H···O=C hydrogen bond [37] [d(N2···O1)= 2.693(4) Å, ∠(N2–H···O1)= 142º(4)] which forms a pseudo-six-membered ring. One of the ester residues is in plane with the phenyl hydrazon moiety (r.m.s. deviation for all non-H atoms 0.060Å) whereas the other one is significantly twisted (80.6º) out of this plane. The molecules lie in planes parallel to (1 4 4), but no pi-stacking is observed between the aromatic rings. There are, instead, N···N short contacts of 3.314 and 3.364 Å between molecules related by (1-x,1-y,1-z).

3.3-Molecular and crystal structure and topology of the electron density.

In order to characterize the intermolecular interaction network that could be expected, positions of hydrogen atoms were optimized at the B3LYP/6-31G(d,p) level and then an AIM topological analysis was performed on the resulting electron density. Relevant topologic and geometrical parameters of all symmetrically nonequivalent interactions are reported in Table 3. As expected, if the value of the electron density at the critical point or the positive eigenvalue of the Laplacian are taken as indicators of their strengths [38], C–H···O interactions in the title compound spread in a very broad range of interaction energies. On the other hand, there is a rather direct correlation between interaction strength and geometry, directionality being no evident even for some of the strongest ones (schematically shown in Figure 3), an indication that electrostatic contributions are not dominant.
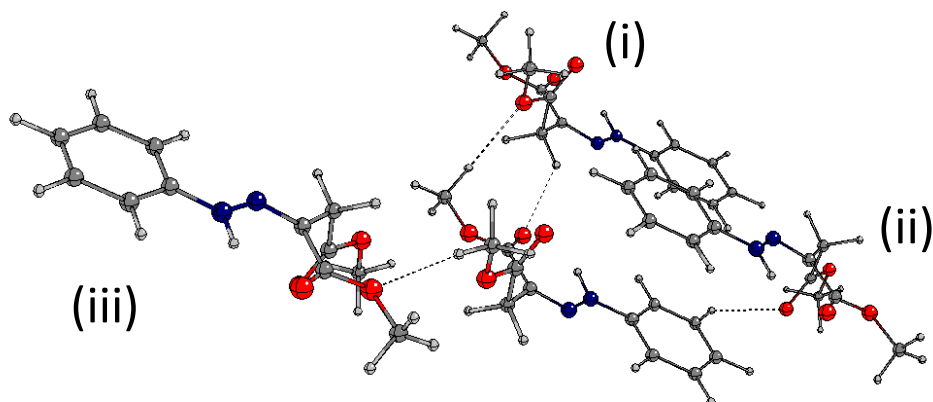
Figure 3. Schematic representation of the most relevant C–H···O interactions. Between parenthesis symmetry operation generating the neighbor molecule (i: -1+x,y,z ; ii: 1-x,-y,1-z ; iii: 2-x,1-y,-z ; iv: 2-x,-y,-z ; v: 1-x,1-y,-z ; vi: -x,1-y,1-z ; vii: 2-x,-y,1-z ; viii: -1+x,1+y,z ; ix: 1-x,1-y,-z).

Table 3. Topological parameters (atomic units) of the crystal and isolated molecule (3,-1) critical points (electron density (ρ), Laplacian ($\nabla^2\rho$) and positive curvature (λ_3)) and geometrical parameters (Å and °) of the corresponding interactions.

	ρ	$\nabla^2\rho$	λ_3	$d_{H\cdots O}$	$\theta_{D–H\cdots O}$
INTRAMOLECULAR[a]					
$H_2\cdots O_1$	0.0302	0.0951	0.1732	1.921	130.1
INTERMOLECULAR[b]					

$H_{3C}\cdots O_4$(i)	0.0101	0.0315	0.0526	2.444	166.2
$H_{25}\cdots O_3$(ii)	0.0084	0.0292	0.0453	2.518	140.2
$O_1\cdots H_{4B}$(i)	0.0080	0.0286	0.0434	2.524	133.4
$H_{6A}\cdots O_2$(iii)	0.0072	0.0251	0.0389	2.578	168.51
$H_{6B}\cdots O_3$(iv)	0.0051	0.0207	0.0292	2.719	125.2
$O_3\cdots H_{3A}$(v)	0.0043	0.0167	0.0234	2.840	128.38
$O_1\cdots H_{26}$(v)	0.0032	0.0130	0.0182	2.932	133.5
$H_{24}\cdots O_4$(vi)	0.0031	0.0123	0.0172	3.007	141.3
$H_{3A}\cdots O_3$(vii)	0.0028	0.0119	0.0155	3.013	137.1
$H_{6A}\cdots O_2$(viii)	0.0024	0.0105	0.0133	3.123	125.0

[a]: crystal (first line) and isolated molecule in the crystal geometry (second line). [b]: atom belonging to the reference molecule on the left of the interaction symbol. Between parenthesis symmetry operation generating the neighbor molecule (i: -1+x,y,z ; ii: 1-x,-y,1-z ; iii: 2-x,1-y,-z ; iv: 2-x,-y,-z ; v: 1-x,1-y,-z ; vi: -x,1-y,1-z ; vii: 2-x,-y,1-z ; viii: -1+x,1+y,z ; ix: 1-x,1-y,-z).

In spite of the *a priori* apparently favorable conditions for the C–H$\cdots$O interactions to be formed, they represent less than one third of the whole set of 33 symmetrically non equivalent close shell interactions characterized in the crystal through the topological properties of the corresponding (3,-1) critical points. Though a quantitative estimation of the relative contribution of the hydrogen bond like interactions to the crystal stability can hardly be made on the basis of electron density topological properties, a prevalence of non directional dispersive contributions can certainly be expected. The role of C–H$\cdots$O interactions in crystal packing can better be inferred from a structural analysis in terms of substructures. Though arbitrary, the centrocymmetric molecular pair generated by symmetry operation (1-x,-y,1-z) seems to be a very natural choice as a starting point. The molecules in this pair are linked each other by a symmetric pair of $H_{25}\cdots O_3$ interactions (see Table 3 and Figure 4). Interactions $H_{3C}\cdots O_4$ and $O_1\cdots H_{4B}$ and

their symmetric counterparts connect molecular pairs along a axis, forming infinite chains, as shown in Figure 4. Chains are linked each other by $H_{6A} \cdots O_2$ interactions. As illustrated in Figure 5, the network consisting of these four C–H$\cdots$O interactions give rise to rather compact layers parallel to the (0 1 1) plane, the most relevant C–H$\cdots$O interaction acting between adjacent layers being the $H_{6B} \cdots O_3$ (see Figure 5). In summary, even if secondary as regards crystal stability, C–H$\cdots$O interactions would have a leading role in the formation of specific patterns.
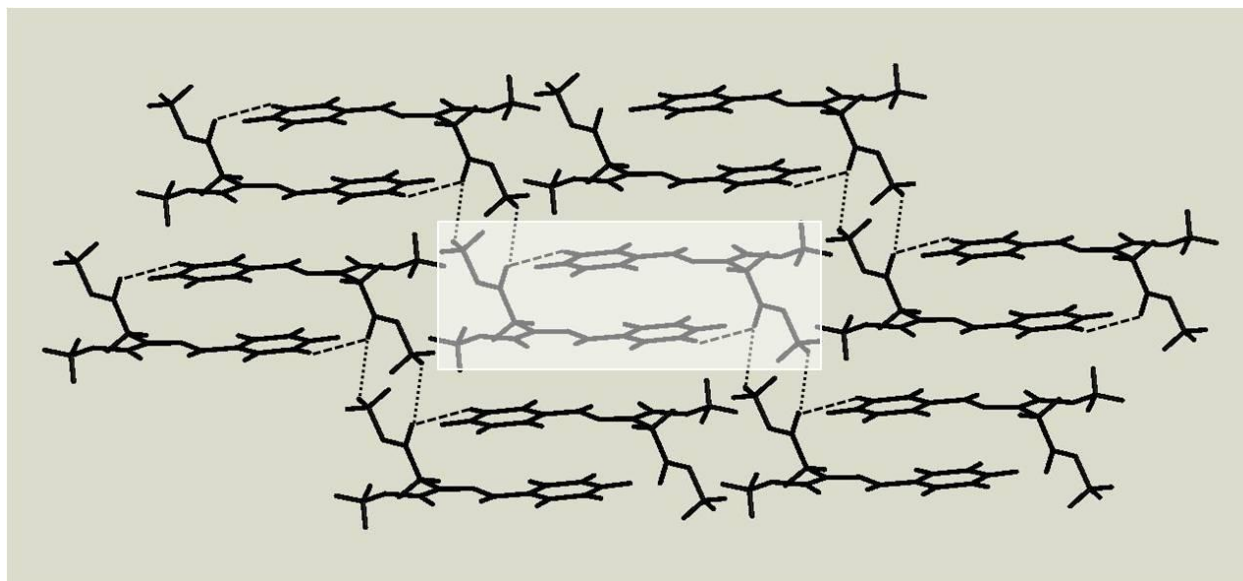
Figure 4. Crystal view along a axis showing the $H_{25} \cdots O_3$ (----) and $H_{6B} \cdots O_3$ (   ) interactions. Highlighted in the center a centrosymmetric pair representing one infinite chain.
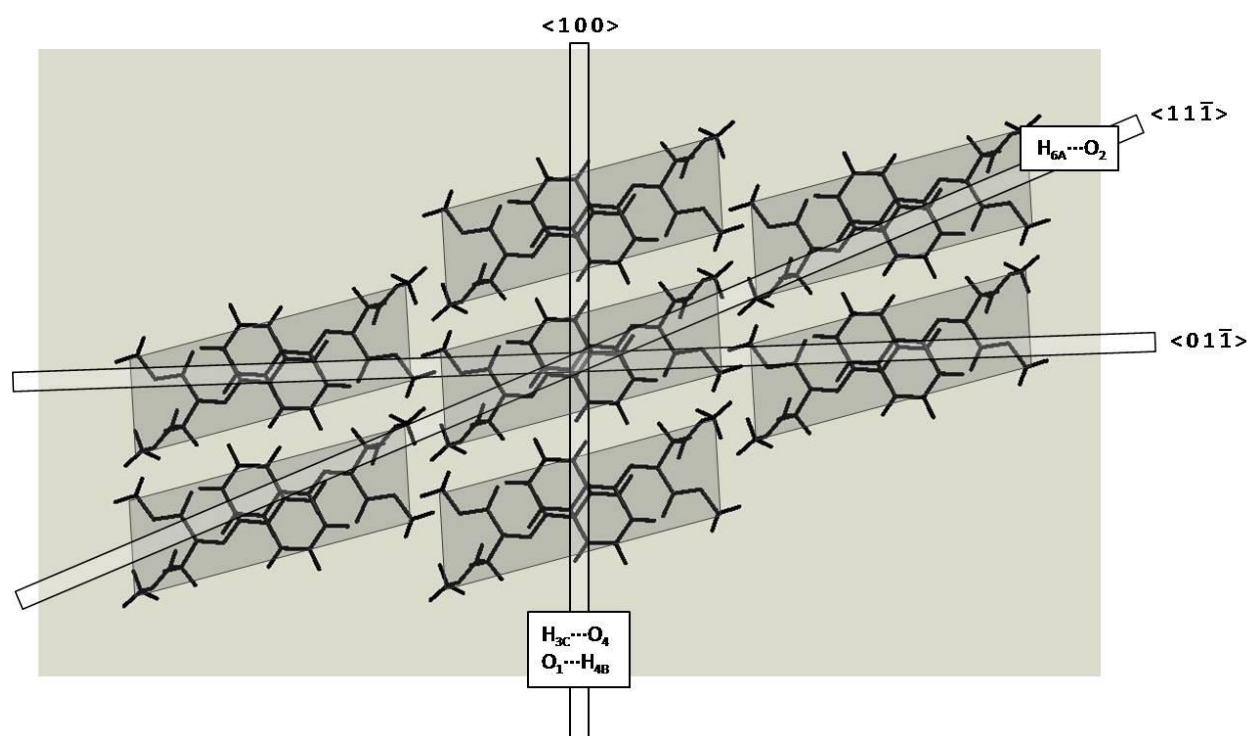
Figure 5. Top view of one of the layers parallel to the (0 1 1) plane. Shaded parallelograms stand for evidencing centrosymmetric molecule pairs. Narrow rectangles labeled <u v w> are included to ease visualization interaction directions.

The existence of an intramolecular N−H···O interaction is confirmed on topologycal grounds. Values of the relevant parameters are reported in Table 3. The interaction can be classified as a resonant assisted hydrogen bond (RAHB) [39] with a rather long H···O distance. Morevoer, the particular fact of having a molecule with two carboxymethyl groups allows to obtain evidence on the resonance mechanism from direct comparison between topological features of the covalent bonds involved. The value of the electron density at the critical point characterizing the C2=O1 bond (0.4025 a.u.) is in fact somewhat smaller than that at the corresponding C5=O3 bond (0.4171 a.u.) but the most relevant indication is the sensible difference in the Laplacian (0.2232 a.u. and 0.3900 a.u., respectively). Some influence of the

resonance on the other groups taking part in the pseudo six-membered ring can also be expected, but obtention of topological evidence would not be straightforward. Concomitantly, some differences in the vibrational behavior of the two carboxymethyl groups could probably be directly characterized, but RAHB influence on other vibrational modes could only be inferred from comparison with related systems [40]. Intramolecular hydrogen bond could also be responsible for the fact that among all motifs carboxymethyl groups usually form each other in molecular crystals [41], only an $R^2_2(10)$ loop can be identified in the crystal.

3.4-Vibrational spectroscopy.

The FTIR and FT-Raman spectra were recorded in the solid phase, as shown in Figure 6. The observed wavenumbers and those calculated at the B3LYP/6-311++G(d,p) level for the most stable form are given as Supplementary Material (Table S7), together with an assignment of the bands as determined from the normal coordinate analysis. When the experimental and the computed infrared spectra for the isolated molecule is compared, it is observed that the qualitative agreement is rather poor, especially when the absorption intensities are considered. It is well-known that the occurrence of intermolecular interactions prevents the interpretation of the experimental spectra on the basis of a single vacuum isolated model, but the whole crystal needs to be considered [42]. Thus, periodic density functional theory (DFT) calculations were applying to investigate the vibrational properties of the title compound in the crystalline phase. The qualitative agreement between the computed and experimental infrared espectra is illustrated on Figure 7 and the computed wavenumbers are also given in Table S7. Because the crystal is centrosymmetric (triclinic space *P*-1), only the modes with A_u symmetry are active in the infrared spectrum.

The proposed assignment is in good agreement with the reported data for related species [43, 44]. Special attention was dedicated to the band assignment of the normal modes associated with the hydrazone group. Thus, the ν(N–H) stretching mode is observed as a weak absorption at 3268 cm^{-1} in the infrared spectrum. This frequency value is lower than that observed for related –C=N–NH–, tipically at 3350 cm^{-1} [9, 44]. It is plausible that the intramolecular N–H⋯O=C hydrogen bond affects the force constant of the hydrozone group. The joint analysis of the ν(C=O) stretching vibration region is of main interest for analyzing the presence of the intramolecular hydrogen bond [45]. Two strong absrorptions are observed at 1739 and 1688 cm^{-1} in the infrared spectrum, with a counterpart at 1689 cm^{-1} in the Raman spectrum. Periodic quantum chemical calculations computed the ν(C=O) values of 1782 and 1737 cm^{-1} for the ν(C5=O3) and ν(C2=O1), respectively. Consequently, it becomes clear that the ν(C=O) red-shift of ca. 51 cm^{-1} experimentally observed between the two esther groups denotes the influence of the N–H⋯O=C intramolecular hydrogen bond in th –O2C2=O1– moiety. It is interesting noticing that the differences in the force constants associated with the ν(C5=O3) and ν(C2=O1) stretching modes observed in the vibrational spectra are in perfect agreement with the results from the topological analysis and the bond distances already discussed.

In the region between 1650-1400 cm^{-1} the characteristic signals corresponding to the C=C stretching are observed in both, the IR and Raman spectra. Superimposed to this features, an absorption observed as a broad band of medium internsity at 1562 cm^{-1} in the infrared spectrum, with a counterpart at 1553 cm^{-1} in Raman, is assigned to the mixed normal mode consisting predominantly of the ν(C1=N) stretching and the δ(N–H) in plane deformation

internal coordinates, with nearly equal contribution, as deduced from the PED analysis. This mode is characteristic for the occurrence of the hydrazo tautomer in the solid phase.

Medium intensity absorptions at 1266 and 1211 cm^{-1} can be observed in the infrared spectrum (with weak counterparts at 1268 and 1214 cm^{-1}, respectively, in the Raman spectrum) are assigned to the antisymmetric and symmetric motion of the C1–C stretching coordinates. The intense infrared absorptions expected for the C–O stretching modes of the ester moieties [46] appear at 1198 cm^{-1} (1192 cm^{-1} in Raman) and 1145 cm^{-1} (1139 cm^{-1} in Raman) for the C5–O4 and C2–O2, respectively.

The ν(N–N) stretching is clearly observed in the Raman spectrum as a medium intensity signal at 1174 cm^{-1}, in good agreement with the computed value (1208 cm^{-1}). For the hydrazine molecule, N_2H_4, this normal mode is reported at 1077 cm^{-1} in the gas phase (the exact value is 1077.24056(82) cm^{-1} from high resolution infrared spectroscopy) [47]. The higher frequency observed for the studied hydrazone species indicates a partial nitrogen-nitrogen double bond, a point that will be further discussed in the next section.
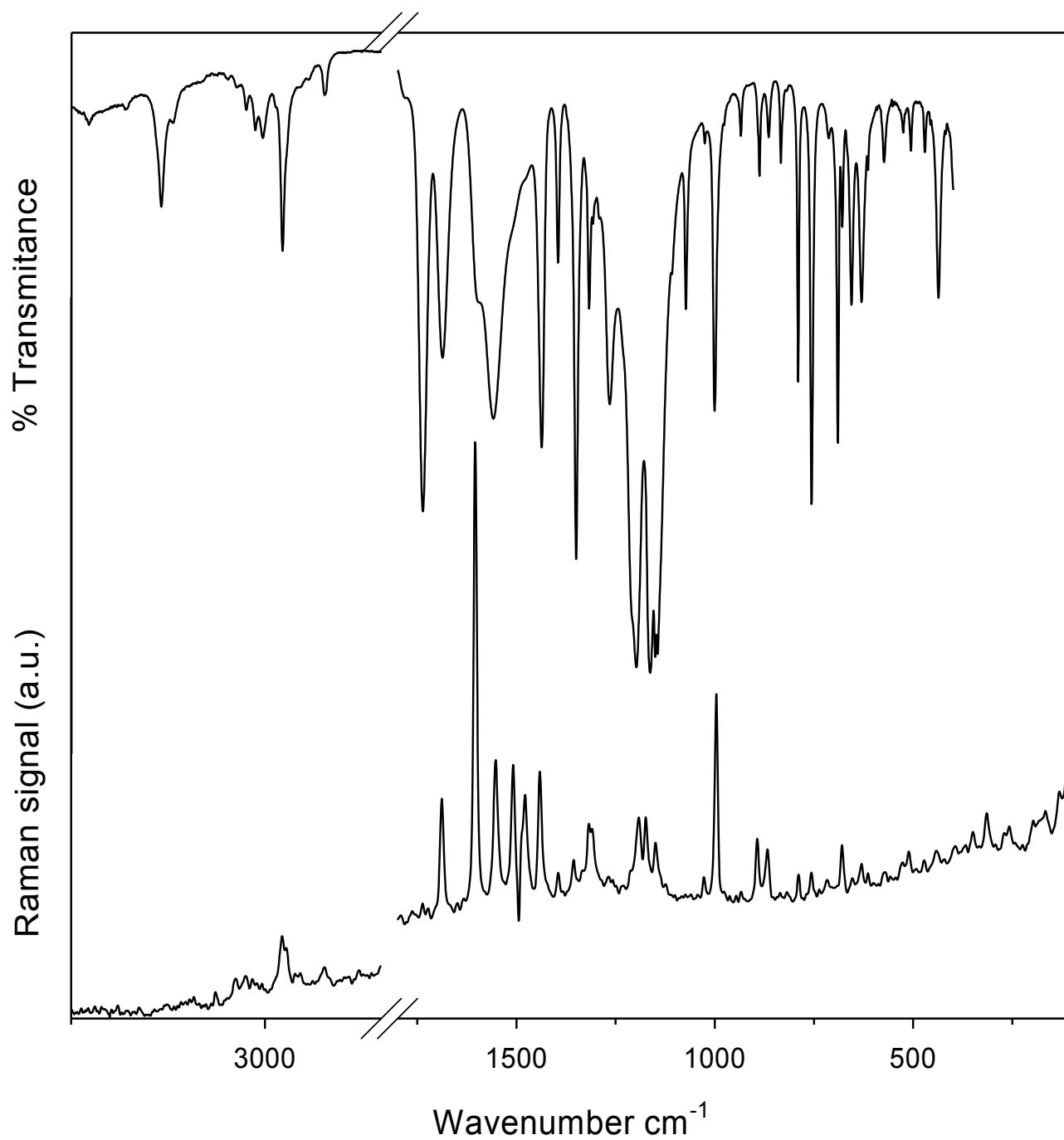
Figure 6. Infrarred (in KBr pellet) and Raman spectra for the solid phase of the title species.
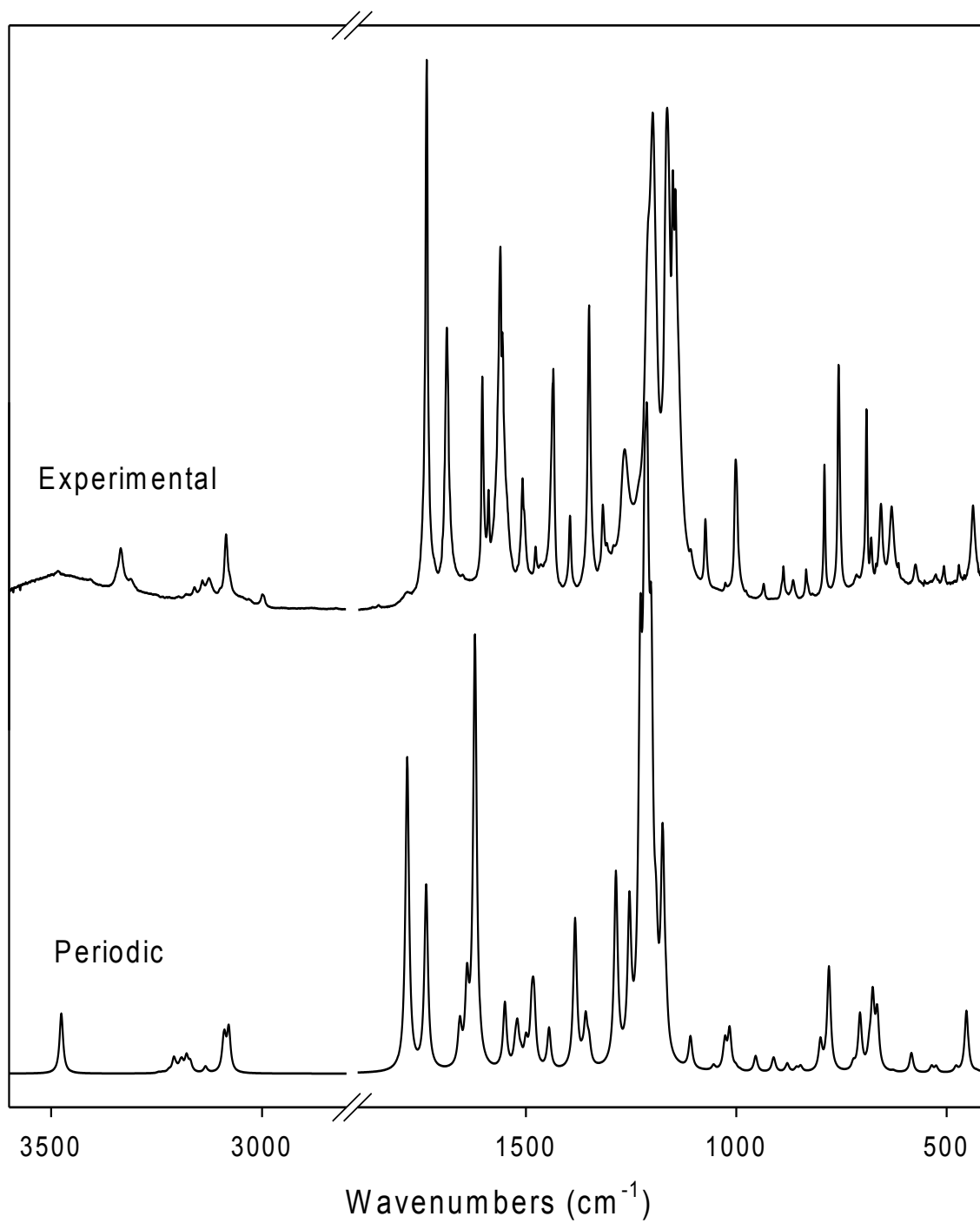
Figure 7. Comparison between the experimental and computed infrared spectra. Periodic density functional theory (DFT) calculations at the B3LYP/6-31G(d,p) was used.

3.5-Natural Bond Orbital Analysis.

The Natural Bond Orbital (NBO) population analysis allow for the calculations of donor→ acceptor interactions estimated by the second order perturbation theory [20]. In particular, the electrostatic contribution for "classical" C=O···H–N hydrogen bonds [48], can be associated with the partial transfer of a lone pair of electrons of the oxygen atom to the N–H antibonding orbital [49, 50]. Such a hyperconjugative interaction can operate between remote orbitals determinaning the conformational landscape of simple molecules [51, 52], as well as the backbone conformation of peptides [53]. For instance, the lpO→ σ*(N–H) remote orbital interaction for benzenesulfonylamin acetamide molecule were computed to be as much as 9.5 kcal/mol [54]. Recently, we also demonstrate that a lpO→ σ*(N–H) remote interaction is responsible for the "*S*-conformation" largely found in 1-acyl thioureas [55, 56]. For the compound here studied, a representation of the lpO1→ σ*(N2–H) remote interaction between the C2=O1 carbonyl and amidate N2–H groups is given in Figure 8. The stabilization energies, $E_{i,j}^{(2)}$, associated with this hyperconjugative interaction is obtained as 9.88 kcal/mol. The hyperconjugative interaction increases the electronic population of the σ*(N2–H) orbital (0.050 **e**).

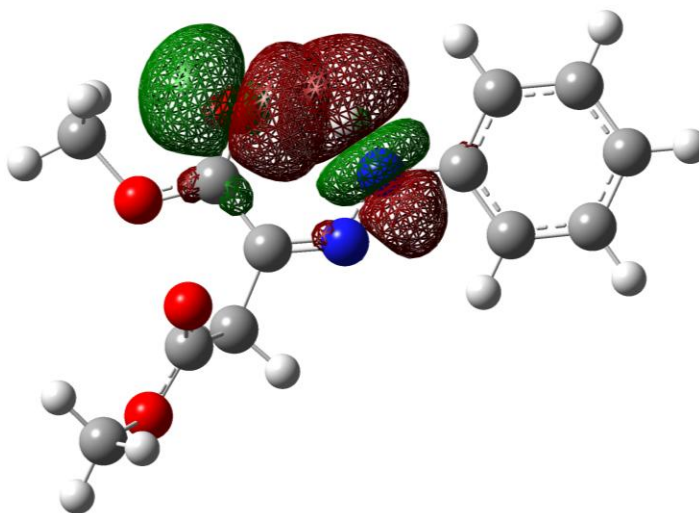**Figure 8.** 3D representation of the remote lpO1→ σ*(N2–H) NBOs overlap responsible for the N–H···O=C intramolecular hydrogen bond.

The NBO analysis also accounts for other interesting electronic properties of the central –C(O)C=NNH– moiety . The presence of a pure p-type [lp_p(N2)] lone pair on the N2–H nitrogen is defined by its exclusive $2p_z$ orbital occupancy, whereas a sp^2 hybrid [s(30.9%), p(69.1%)] better describes the valence electron of the nitrogen atom of the C=N1- group. The p-type orbital displays an electron occupancy of 1.60 **e**, indicating the electron-donating capacity. Delocalizing interactions evaluated by a second-order perturbation approach reveals that this orbital contributes to a strong resonance interactions with the C1=N1 double bond as well as with the π system of the phenyl ring. The computed $E^{(2)}$ energy values for the lp_p(N2)→ $π^*$(C1=N1) and lp_p(N2)→ $π^*$(C=C) interactions are 48.4 and 34.6 kcal/mol, respectively. This strong donor→ acceptor overlap between the lp_p(N2) and $π^*$(C1=N1) orbitals can be associated with resonance structure having a partial double bond character for the N1–N2 bond. This picture is in

qualitative agreement with the high frequency value experimentally observed for the ν(N–N) stretching in the studied compound.

The π resonance system is extended through the π(C1=N1)$\rightarrow \pi^*$(C2=O1) interaction, which amount to 16.3 kcal/mol. Finally, the lpπO2$\rightarrow \pi^*$(C2=O1) donor-aceptor interaction within the –O2C2=O1– group is computed at 46.7 kcal/mol. As a consequences, the π^*(C2=O1) corresponds to the LUMO and the occupancy of this formally "vacant" orbital attains as much as 0.314 **e**. It should be noted that the molecule has a second ester group –O4C5=O3–. However, it is clear that the resonance interaction with the –C=N–NH– system is precluded because the presence of the –CH$_2$– group, which acts as a separator between the donor and acceptor. Thus only the lpπO4$\rightarrow \pi^*$(C5=O3) interaction is observed within this group, with a value of 46.2 kcal/mol. This loss of electronic delocalization is also reflected in higher occupancy of the π^*(C5=O3) (0.215 **e**) as compared with π^*(C=O1). According to the usual resonance scheme, more efficient lpO$\rightarrow \pi^*$(C=O) interactions are associated with longer C=O and shorter C–O bond distances of the ester moieties, similar to those observed for related compounds [46, 57, 58]. The computed donor$\rightarrow$ acceptor values agree with the tendency observed for C–O and C=O bond distances, with experimental bond length values of 1.336(1) and 1.341(1) Å for the C2–O2 and C4–O5, respectively, whereas the C=O double bond distances amounts to 1.220 (C2=O1) and 1.203 (C5=O3) Å.

4-Conclusions

The synthesis of a carbonyl-bearing hydrazone compound was successfully achieved by the reaction between phenyl hydrazine with dimethylacetylene dicarboxylate. The X-ray structure determination and the vibrational analysis agree with the fact that the molecule is present in the crystal as the hydrazone tautomer. Quantum chemical calculations at the B3LYP/6-311++G(d,p) reproduce this observation, the hydrazo E syn form being the most stable structure for the isolated molecule.

A intramolecular N–H···O=C hydrogen bond between the carbonyl (–C=O) bond and the hydrazone –C=N–NH– group is present in the crystal and was characterized in terms of topological and NBO analysis. In particular, the stabilization energy, $E_{i,j}^{(2)}$, associated with the lpO1→ σ*(N2–H) remote interaction amount to 9.88 kcal/mol. To the best of our knowledge, this is the first quantitative explanation for such a strong remote interaction involving hydrazone compounds.

The vibrational IR and Raman spectra are well explained by the presence of the hydrazone tautomer. Periodic quantum chemical calculations reproduces the infrared spectrum in excelent agreement. The carbonyl stretching region shows two bands with ν(C=O) shift of ca. 51 cm^{-1} between the two esther groups, the low frequency one assigned to C=O group affecting by the N–H···O=C intramolecular hydrogen bond. The ν(N–N) stretching is observed in the Raman spectrum as a medium intensity signal at 1174 cm^{-1}, in good agreement with the computed value (1208 cm^{-1}), reinforcing the proposed hydrazone structure.

The topological analysis of the periodic system electron density provided evidences on the role of the C–H···O interactions in the stablishement of the crystal pattern, though they are of secondary importance as regards crystal stability.

5-Acknowledgments

6- Supplementary data

Atomic coordinates, equivalent isotropic displacement coefficients, geometrical parameters and anisotropic displacement parameters are given in Tables S1-S4, respectively. Tables S5 and S6 list the torsion angles and hydrogen bond geometrical parameters, respectively. Table S7 gives FTIR and FT-Raman experimental and computed data for the studied compound, together with the normal mode assignment. The ^{1}H and ^{13}C NMR spectra are shown in Figures S1 and S2, respectively.

7-References

[1] N.P. Belskaya, W. Dehaen, V.A. Bakuleva, Synthesis and properties of hydrazones bearing amide, thioamide and amidine functions, Arkivoc, 2010 (2010) 275-332.

[2] G. Verma, A. Marella, M. Shaquiquzzaman, M. Akhtar, M. Ali, M. Alam, A review exploring biological activities of hydrazones, J. Pharm. Bioallied Sci., 6 (2014) 69-80.

[3] E.G.J. Staring, G.L.J.A. Rikken, C.J.E. Seppen, S. Nijhuis, A.H.J. Venhuizen, Organic materials for frequency doubling, Adv. Mat., 3 (1991) 401-403.

[4] A. Manimekalai, N. Saradhadevi, A. Thiruvalluvar, Molecular structures, spectral and computational studies on nicotinohydrazides, Spectrochim. Acta, 77A (2010) 687-695.

[5] C. Ravikumar, I.H. Joe, V.S. Jayakumar, Charge transfer interactions and nonlinear optical properties of push-pull chromophore benzaldehyde phenylhydrazone: A vibrational approach, Chem. Phys. Lett., 460 (2008) 552-558.

[6] L. Arrue, X. Zarate, S. Schott-Verdugo, E. Schott, Substituted phenylhydrazono derivatives of curcumin as new ligands, a theoretical study, Chem. Phys. Lett., 623 (2015) 42-45.

[7] D. Debnath, S. Roy, B.-H. Li, C.-H. Lin, T.K. Misra, Synthesis, structure and study of azo-hydrazone tautomeric equilibrium of 1,3-dimethyl-5-(arylazo)-6-amino-uracil derivatives, Spectrochim. Acta, 140A (2015) 185-197.

[8] P. Rawat, R.N. Singh, Eco-friendly synthesis, spectral and computational study of Pyrrole-2-carboxaldehyde salicylhydrazone (PCSH) for its application, J. Mol. Struct., 1100 (2015) 105-115.

[9] N. Galić, I. Brođanac, D. Kontrec, S. Miljanić, Structural investigations of aroylhydrazones derived from nicotinic acid hydrazide in solid state and in solution, Spectrochim. Acta, 107A (2013) 263-270.

[10] R. Bhaskar, N. Salunkhe, A. Yaul, A. Aswar, Bivalent transition metal complexes of ONO donor hydrazone ligand: synthesis, structural characterization and antimicrobial activity, Spectrochim. Acta, 151 (2015) 621−627.

[11] A. Alimmari, B. Božić, D. Mijin, A. Marinković, N. Valentić, G. Ušćumlić, Synthesis, structure and solvatochromic properties of some novel 5-arylazo-6-hydroxy-4-(4-methoxyphenyl)-3-cyano-2-pyridone dyes: Hydrazone-azo tautomeric analysis, Arabian J. Chem., 8 (2015) 269-278.

[12] T.F.d. Silva, W.B. Júnior, M.S. Alexandre-Moreira, F.N. Costa, C.E.d.S. Monteiro, F.F. Ferreira, R.C.R. Barroso, F. Noël, R.T. Sudo, G. Zapata-Sudo, L.M. Lima, E.J. Barreiro, Novel Orally Active Analgesic and Anti-Inflammatory Cyclohexyl-N-Acylhydrazone Derivatives, Molecules, 20 (2015) 3067-3088.

[13] A.B. Lopes, E. Miguez, A.E. Kümmerle, V.M. Rumjanek, C.A.M. Fraga, E.J. Barreiro, Characterization of Amide Bond Conformers for a Novel Heterocyclic Template of N-acylhydrazone Derivatives, Molecules, 18 (2013) 11683-11704.

[14] I.M. Kenawi, M.H. Elnagdi, DFT and FT-IR analyses of hydrogen bonding in 3-substistuted-3-oxo-arylhydrazonopropanenitriles, Spectrochim. Acta, 65A (2006) 805-810.

[15] D. Sarıgöla, D. Yüksela, G. Okayb, A. Uzgören-Baran, Synthesis and structural studies of acyl hydrazone derivatives having tetrahydrocarbazole moiety, J. Mol. Struct., 1086 (2015) 146-152.

[16] R. Benassi, A. Benedetti, F. Taddei, R. Cappelletti, D. Nardi, A. Tajana, Conformational analysis of hydrazones. 1H dynamic nuclear magnetic resonance and solvent effects in aryl- and 2-furylaldehyde ethylaminoacetylhydrazones, Org. Magn. Res., 20 (1982) 26-30.

[17] W. You, H.-Y. Zhu, W. Huang, B. Hu, Y. Fan, X.-Z. You, The first observation of azo-hydrazone and cis-trans tautomerisms for disperse yellow dyes and their nickel(ii) and copper(ii) complexes, Dalton Trans., 39 (2010) 7876-7880.

[18] W. Jamil, S. Solangi, M. Ali, K.M. Khan, M. Taha, M.Y. Khuhawar, Syntheses, characterization, in vitro antiglycation and DPPH radical scavenging activities of isatin salicylhydrazidehydrazone and its Mn (II), Co (II), Ni (II), Cu (II), and Zn (II) metal complexes, Arabian J. Chem., *In press*, 2015, doi:10.1016/j.arabjc.2015.02.015.

[19] N. Zohreh, A. Alizadeh, Simple and efficient one-pot synthesis of N-phenyl-3,5-difunctionalized pyrazoles, Tetrahedron, 67 (2011) 4595-4600.

[20] A.E. Reed, L.A. Curtiss, F. Weinhold, Intermolecular Interactions from a Natural Bond Orbital, Donor-Acceptor Viewpoint, Chem. Rev., 88 (1988) 899-926.

[21] M.J. Frisch, G.W. Trucks, H.B. Schlegel, G.E. Scuseria, M.A. Robb, J.R. Cheeseman, J.A. Montgomery Jr., T. Vreven, K.N. Kudin, J.C. Burant, J.M. Millam, S.S. Iyengar, J. Tomasi, V. Barone, B. Mennucci, M. Cossi, G. Scalmani, N. Rega, G.A. Petersson, H. Nakatsuji, M. Hada, M. Ehara, K. Toyota, R. Fukuda, J. Hasegawa, M. Ishida, T. Nakajima, Y. Honda, O. Kitao, H. Nakai, M. Klene, X. Li, J.E. Knox, H.P. Hratchian, J.B. Cross, C. Adamo, J. Jaramillo, R. Gomperts, R.E. Stratmann, O. Yazyev, A.J. Austin, R. Cammi, C. Pomelli, J.W. Ochterski, P.Y. Ayala, K. Morokuma, G.A. Voth, P. Salvador, J.J. Dannenberg, V.G. Zakrzewski, S. Dapprich,

A.D. Daniels, M.C. Strain, O. Farkas, D.K. Malick, A.D. Rabuck, K. Raghavachari, J.B. Foresman, J.V. Ortiz, Q. Cui, A.G. Baboul, S. Clifford, J. Cioslowski, B.B. Stefanov, G. Liu, A. Liashenko, P. Piskorz, I. Komaromi, R.L. Martin, D.J. Fox, T. Keith, M.A. Al-Laham, C.Y. Peng, A. Nanayakkara, M. Challacombe, P.M.W. Gill, B. Johnson, W. Chen, M.W. Wong, C. Gonzalez, J.A. Pople, Gaussian 03, in, Gaussian, Inc., Pittsburgh PA, 2003.

[22] M.J. Frisch, J.A. Pople, J.S. Binkley, Self-consistent molecular orbital methods 25. Supplementary functions for Gaussian basis sets, J. Chem. Phys., 80 (1984) 3265-3269.

[23] M.H. Jamróz, Vibrational Energy Distribution Analysis (VEDA): Scopes and limitations, Spectrochim. Acta, 114A (2013) 220-230.

[24] M.H. Jamróz, Vibrational Energy Distribution Analysis VEDA 4, in, Warsaw, 2004.

[25] R. Dovesi, R. Orlando, B. Civalleri, C. Roetti, V.R. Saunders, C.M. Zicovich-Wilson, CRYSTAL: a computational tool for the ab initio study of the electronic properties of crystals, Z. Kristallogr., 220 (2005) 571-573.

[26] R. Dovesi, V.R. Saunders, C. Roetti, R. Orlando, C.M. Zicovich-Wilson, F. Pascale, B. Civalleri, K. Doll, N.M. Harrison, I.J. Bush, P. D'Arco, M. Llunell, CRYSTAL09 User's Manual, University of Torino, Torino, (2009).

[27] C. Gatti, TOPOND 98 User's Manual, CNR-ISTM, Milano., (1999).

[28] in, Stoe & Cie. X-Area. Area-Detector Control and Integration Software, Stoe & Cie, Darmstadt, Germany, 2001.

[29] G. Sheldrick, A Short History of SHELX, Acta Crystallogr., A64 (2008) 112-122.

[30] P.H. Cebrowski, J.-G. Roveda, J. Moran, S.I. Gorelsky, A.M. Beauchemin, Intermolecular Cope-type hydroamination of alkynes using hydrazines, Chem. Comm., (2008) 492-493.

[31] V.I. Minkin, A.V. Tsukanov, A.D. Dubonosov, V.A. Bren, Tautomeric Schiff bases: Iono-, solvato-, thermo- and photochromism, J. Mol. Struct., 998 (2011) 179-191.

[32] R. Benassi, F. Taddei, Theoretical study of conformational changes in simple hydrazones, J. Chem. Soc., Perkin Trans. 2, (1985) 1629-1632.

[33] W. Kuznik, M.N. Kopylovich, G.I. Amanullayeva, A.J.L. Pombeiro, A.H. Reshak, K.T. Mahmudov, I.V. Kityk, Role of tautomerism and solvatochromism in UVâ€"VIS spectra of arylhydrazones of Î²-diketones, J. Mol. Liq., 171 (2012) 11-15.

[34] A.R.E. Carey, S. Eustace, R.A.M. O'Ferrall, B.A. Murray, Keto-Enol and imine-enamine tautomerism of 2-, 3- and 4-phenacylpyridines, J. Chem. Soc., Perkin Trans. 2, (1993) 2285-2296.

[35] F.H. Allen, O. Kennard, D.G. Watson, L. Brammer, A.G. Orpen, R. Taylor, Tables of bond lengths determined by X-ray and neutron diffraction. Part 1. Bond lengths in organic compounds, J. Chem. Soc., Perkin Trans. 2, (1987) S1-S19.

[36] M.K. Usha, S. Shetty, B. Kalluraya, R. Kant, V.K. Gupta, D. Revannasiddaiah, Dimethyl 2-[2-(2,4,6-trichlorophenyl)hydrazin-1-ylidene]butanedioate, Acta Crystallogr., E70 (2014) o13.

[37] R. Taylor, O. Kennard, W. Versichel, The geometry of the N-H...O=C hydrogen bond. 3. Hydrogen-bond distances and angles, Acta Crystallogr., B40 (1984) 280-288.

[38] E. Espinosa, M. Souhassou, H. Lachekar, C. Lecomte, Topological analysis of the electron density in hydrogen bonds, Acta Crystallogr., B55 (1999) 563-572.

[39] T. Steiner, The Hydrogen Bond in the Solid State, Angew. Chem. Int. Ed., 41 (2002) 48-76.

[40] A.R. Nekoei, M. Vatanparast, An intramolecular hydrogen bond study in some Schiff bases of fulvene: a challenge between the RAHB concept and the [sigma]-skeleton influence, New J. Chem., 38 (2014) 5886-5891.

[41] J. Bernstein, M.C. Etter, L. Leiserowitz, The Role of Hydrogen Bonding in Molecular Assemblies, Wiley-VCH Verlag GmbH, 2008.

[42] D. Galimberti, A. Milani, Crystal Structure and Vibrational Spectra of Poly(trimethylene terephthalate) from Periodic Density Functional Theory Calculations, J. Phys. Chem. B, 118 (2014) 1954-1961.

[43] A.A.M. Belal, M.A. Zayed, M. El-Desawy, S.M.A.H. Rakha, Structure investigation of three hydrazones Schiff-bases by spectroscopic, thermal and molecular orbital calculations and their biological activities, Spectrochim. Acta, 138A (2015) 49-57.

[44] Y. Kaya, C. Icsel, V.T. Yilmaz, O. Buyukgungor, Structural, spectroscopic and quantum chemical studies of acetyl hydrazone oxime and its palladium(II) and platinum(II) complexes, J. Mol. Struct., 1095 (2015) 51-60.

[45] M.S.M. Yusof, R.H. Jusoh, W.M. Khairul, B.M. Yamin, Synthesis and characterisation a series of N-(3,4-dichlorophenyl)-N'-(2,3 and 4-methylbenzoyl)thiourea derivatives, J. Mol. Struct., 975 (2010) 280-284.

[46] M.F. Erben, R. Boese, C.O. Della Védova, H. Oberhammer, H. Willner, Toward an Intimate Understanding of the Structural Properties and Conformational Preference of Oxoesters and Thioesters: Gas and Crystal Structure and Conformational Analysis of Dimethyl Monothiocarbonate, CH3OC(O)SCH3, J. Org. Chem., 71 (2006) 616-622.

[47] I. Gulaczyk, M. Kręglewski, A. Valentin, The N-N stretching band of hydrazine, J. Mol. Spectrosc., 220 (2003) 132-136.

[48] G.R. Desiraju, Hydrogen Bridges in Crystal Engineering: Interactions without Borders, Acc. Chem. Res., 35 (2002) 565-573.

[49] I.V. Alabugin, M. Manoharan, S. Peabody, F. Weinhold, Electronic Basis of Improper Hydrogen Bonding: A Subtle Balance of Hyperconjugation and Rehybridization, J. Am. Chem. Soc., 125 (2003) 5973-5987.

[50] K. Gholivand, F. Molaei, Synthesis and structural study of some new phosphorus(v) hydrazide compounds: spectroscopic evidence and a theoretical approach, New J. Chem., 39 (2015) 3747-3757.

[51] A.J. Lopes Jesus, M.T.S. Rosado, I. Reva, R. Fausto, M.E.S. Eusébio, J.S. Redinha, Structure of Isolated 1,4-Butanediol: Combination of MP2 Calculations, NBO Analysis, and Matrix-Isolation Infrared Spectroscopy, J. Phys. Chem. A, 112 (2008) 4669-4678.

[52] J.R. Lucena, A. Sharma, I.D. Reva, R.M.C.U. Araújo, E. Ventura, S.A. do Monte, C.F. Braga, M.N. Ramos, R. Fausto, Matrix Isolation FTIR Spectroscopic and Theoretical Study of 3,3-Dichloro-1,1,1-Trifluoropropane (HCFC-243), J. Phys. Chem. A, 112 (2008) 11641-11648.

[53] J.J. Koivisto, E.T.T. Kumpulainen, A.M.P. Koskinen, Conformational ensembles of flexible [small beta]-turn mimetics in DMSO-d6, Org. Biomol. Chem., 8 (2010) 2103-2116.

[54] L. Aguilar-Castro, M. Tlahuextl, L.H. Mendoza-Huizar, A.R. Tapia-Benavides, H. Tlahuext, Hydrogen bond studies in substituted N-(2-hydroxyphenyl)--2-[(4-methylbenzenesulfonyl)amino]acetamides ARKIVOC, (2008) 210-226.

[55] A. Saeed, A. Khurshid, J.P. Jasinski, C.G. Pozzi, A.C. Fantoni, M.F. Erben, Competing intramolecular NH···OC hydrogen bonds and extended intermolecular network in 1-(4-chlorobenzoyl)-3-(2-methyl-4-oxopentan-2-yl) thiourea analyzed by experimental and theoretical methods, Chem. Phys., 431-432 (2014) 39-46.

[56] A. Saeed, A. Khurshid, M. Bolte, A.C. Fantoni, M.F. Erben, Intra- and intermolecular hydrogen bonding and conformation in 1-acyl thioureas: An experimental and theoretical approach on 1-(2-chlorobenzoyl)thiourea, Spectrochim. Acta, 143A (2015) 59-66.

[57] M.F. Erben, C.O. Della Védova, R.M. Romano, R. Boese, H. Oberhammer, H. Willner, O. Sala, Anomeric and Mesomeric Effects in Methoxycarbonylsulfenyl Chloride, $CH_3OC(O)SCl$: An Experimental and Theoretical Study, Inorg. Chem., 41 (2002) 1064-1071.

[58] I.V. Alabugin, T.A. Zeidan, Stereoelectronic Effects and General Trends in Hyperconjugative Acceptor Ability of sigma Bonds, J. Am. Chem. Soc., 124 (2002) 3175-3185.

Acyl-substituted Hydrazones

Hyperconjugative
Remote Interaction

Intermolecular interactions
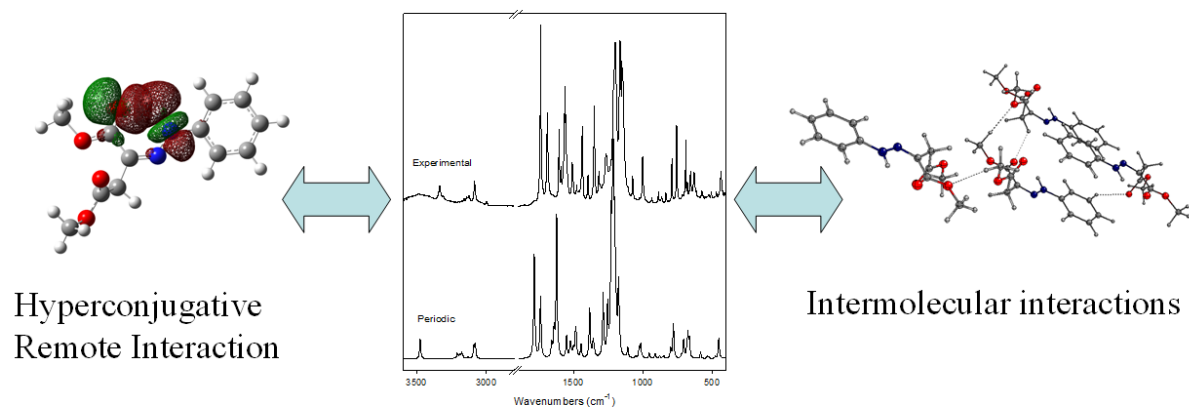
Graphical abstract

Highlights

► Crystal structures and vibrational properties were determined. ► The molecular hydrazone skeleton is planar due to an extended π-bonding delocalization ► The acyl hydrazone group is involved in strong N–H···O=C intramolecular hydrogen bond ► Strong hyperconjugative lpO1→ σ*(N2–H) remote interaction takes place ► Intramolecular N–H···O interaction are described by AIM topological analysis describes.